# Native Electrospray Ionization of Multi-Domain Proteins via a Bead Ejection Mechanism

Nina Khristenko, Frédéric Rosu, Eric Largy, Jérôme Haustant, Cédric Mesmin, Valérie Gabelica

This is the accepted version of a manuscript published in final form as Ghosh D, Rosu F, Gabelica V. Khristenko N, Rosu F, Largy E, Haustant J, Mesmin C, Gabelica V. "Native Electrospray Ionization of Multi-Subunit Therapeutic Proteins via a Bead Ejection Model", J. Am. Chem. Soc. (2023) 145(1), 498-506.
DOI: https://doi.org/10.1021/jacs.2c10762
It may not reflect final changes made by the Editor.

# Native Electrospray Ionization of Multi-Subunit Proteins via a Bead Ejection Mechanism

Nina Khristenko,[a] Frédéric Rosu,[b] Eric Largy,[a] Jérôme Haustant,[c] Cédric Mesmin[c]

& Valérie Gabelica[a,b]*

[a] Univ. Bordeaux, CNRS, INSERM, ARNA, UMR5320, U1212, IECB, F-33600 Pessac, France

[b] Univ. Bordeaux, CNRS, INSERM, IECB, UAR3033, US01, F-33600 Pessac, France

[c] Merck Biodevelopment SAS /An Affiliate of Merck KGaA – Darmstadt, Germany / F- 33650 Martillac, France

* corresponding author: v.gabelica@iecb.u-bordeaux.fr

## Abstract

Native ion mobility mass spectrometry is potentially useful for the biophysical characterization of proteins, as the electrospray charge state distribution and the collision cross section distribution depend on their solution conformation. We examine here the charging and gas-phase conformation of multi-subunit therapeutic proteins comprising globular subunits tethered by disordered linkers. The charge and collision cross section distributions are multimodal, suggesting several conformations in solution, as confirmed by solution hydrogen/deuterium exchange. The most intriguing question is the ionization mechanism of these structures: a fraction of the population does not follow the charged residue mechanism, but cannot ionize by pure chain ejection either. We deduce that a hybrid mechanism is possible, wherein globular subunits are ejected one at the time from a parent droplet. The charge vs. solvent accessible surface area correlations of denatured and intrinsically disordered proteins are also compatible with this "bead ejection mechanism", which we propose as a general tenet of biomolecule electrospray.


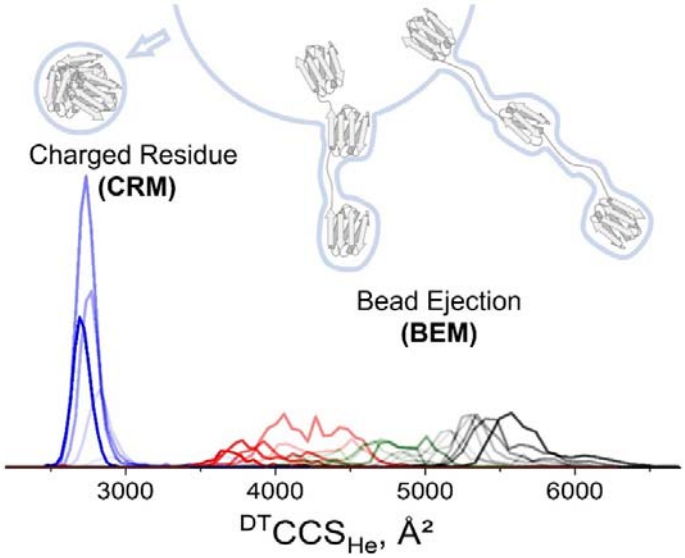

## Introduction

Electrospray is the most widely used ionization method for biomolecule mass spectrometry. But even 35 years after electrospray invention,[1,2] the mechanisms of final ion charging and desolvation are still debated.[3,4] Three limiting cases are usually described: (1) the ion evaporation mechanism (IEM),[5,6] in which intact ions are emitted from the surface of a droplet with a minimal solvent shell, (2) the charged residue mechanism (CRM),[7,8] in which a droplet containing a single analyte and electrolytes evaporates to dryness, and (3) the chain ejection mechanism (CEM),[9] in which a flexible analyte is progressively extruded from the droplet surface as a chain and carries away numerous charges. A charge equilibration along the surface of the protein explains that more charges end up on a protein undergoing the CEM than the CRM.[9]

Globular proteins are usually thought to ionize via the CRM: they adopt charge states close to the Rayleigh limit of electrospray droplets, and end up compact in the gas phase. In contrast, unfolded proteins are supposed to be ionized by the chain ejection mechanism, can reach higher charge states and extended conformations. Yet, denatured or intrinsically disordered proteins typically adopt a wide variety of charge states and gas-phase conformations,[10] which are neither globular nor fully extended. This suggests that an intermediate scenario must exist between the CRM and the CEM to account for biomolecule ionization.[11] We explored this intermediate regime with proteins having a multi-subunit topology, and propose here an ionization process via a bead ejection mechanism.

Recombinant proteins are important therapeutic tools in modern medicine and a major part of FDA-approved drugs, with currently over 240 protein-based therapeutics.[12] Folding into a specific three-dimensional structure is essential for the activity, stability, and safety of therapeutic proteins. The biopharma industry needs biophysical characterization to control the proper structure recovery of a drug, to check the conformational homogeneity during process development, and to verify the batch-to-batch consistency during commercial drug production. Traditional spectroscopic methods make it difficult to analyze co-existing conformations because of signal convolution, and the

separation of fast inter-converting conformers is not always possible. Mass spectrometry approaches, however, give a snapshot of the solution composition by transferring the different conformers to the gas phase, where their shape can be probed by ion mobility spectrometry. One of our objectives was to establish whether this snapshot is faithful to the solution conformational ensembles, and if yes, why?

The electrospray process typically confers fewer charges to folded conformations than to unfolded or disordered proteins.[13–16] Multimodal charge state distributions (CSD) under native conditions can thus reveal multiple co-existing conformations.[15] Ion mobility mass spectrometry (IM-MS) is a complementary method, probing conformational ensembles based on the differential friction of individual conformers with a gas when dragged by an electric field.[17,18] The experimental momentum transfer collision integral (or collisional cross section—CCS) indicates the compactness of the biomolecule. Calculated CCS of candidate structures help assign each conformer family. Charge state ($z$) and collision cross section ($CCS$) are inter-dependent: higher charge states usually have more extended conformations because of increased Coulomb repulsion. The key question is: What determines the number of charges to begin with? Is it solely determined by the solution conformation (the charge being related to the solvent accessible surface area)[19] or do some electrospray-related processes further influence the charging and thus the gas phase conformations? Understanding the electrospray mechanisms is thus important for a reliable interpretation of native IM-MS data for solution biophysics.

## Experimental Section

### Sample preparation

The recombinant proteins 2S, 3S and 4S were produced in the culture broth during the Fed-Batch fermentation of proprietary Pichia pastoris strains. The promoter of the transgenes was the natural AOX1 promoter. The induction of the protein expression was thus done using methanol (Sigma-Aldrich, USA). The recombinant proteins were further purified using a proprietary workflow, including several chromatographic steps. 2S was formulated in L-histidine 1.48 mg/mL and L-histidine monohydrochloride monohydrate 2.193 mg/mL with sucrose 80 mg/mL and polysorbate 20 0.1 mg/mL (Merck KGaA, Darmstadt - Germany). 3S was formulated in 10 mM phosphate buffer with sucrose 8% w/v and polysorbate 80 0.01% v/v (Merck KGaA, Darmstadt - Germany). 4S was formulated in histidine 20 mM and trehalose 8% w/v (Merck KGaA, Darmstadt - Germany). The protein concentration was determined by Amino Acid Analysis using the Dionex ICS-3000 system equipped with the IPAD detector (integrated pulsed amperometric detection). Before MS analyses, the buffer was exchanged to 15 mM or 50 mM ammonium acetate (Sigma-Aldrich, USA) using 0.5-mL Amicon Ultra centrifugal filters (regenerated cellulose, 10,000 molecular weight cut-off; Merck KGaA, Darmstadt - Germany). The filters were first filled with ULC/MS-grade water (Biosolve, France) and centrifuged at 14,000 g for 15 min (Eppendorf 5430R centrifuge), after which the filtrates were discarded. The protein samples (15 mg) and ammonium acetate solution (15 or 50 mM) were then loaded and centrifuged at 14,000 g for 12 min, after which the filtrates were discarded. The same conditions were used three more times to wash the samples with 15 or 50 mM ammonium acetate. Finally, the supernatants were collected into new tubes by inverting the filters and centrifuging them at 2,000 g for 2 min. All steps were carried out at 20°C.

**Ion mobility mass spectrometry**

IM-MS experiments were performed on an Agilent 6560 DTIMS-Q-TOF instrument (Agilent Technologies, Santa Clara, CA), equipped with the dual-ESI source operated in the positive ion mode. The pre-IM conditions were optimized for softness as described elsewhere,[20] and we used the following values: fragmentor = 320 V (in activation experiments, fragmentor = 500 V), trap fill time = 1000 μs, trap release time = 200 μs, trap entrance grid delta = 2 V. The drift tube was filled with helium at 3.89 ± 0.01 Torr (measured by a capacitance diaphragm gauge CDG-500, Agilent Technologies) and 23.5 °C. Each step-field drift tube ion mobility experiment included 5 segments with duration varying from 2 to 7 min, where drift tube entrance voltage was 650 V, 700 V, 800 V, 900, V and 1000 V. The flow rate used with the single syringe or multiple syringes set-up was 3.5 μL/min. The protein was injected at 10 μM concentration in 15 mM or 50 mM aqueous ammonium acetate.

The ESI-L Tuning Mix solution from Agilent Technologies was used to perform the mass calibration. The CCS were measured for various components of Tuning Mix to verify or adjust the gas pressures before and inside the drift tube. Targeted CCS values were the following: $^{DT}CCS_{He}$ = 139.0 Å$^2$ for m/z 622, $^{DT}CCS_{He}$ = 175.5 Å$^2$ for m/z 922, $^{DT}CCS_{He}$ = 208.2 Å$^2$ for m/z 1222, $^{DT}CCS_{He}$ = 238.1 Å$^2$ for m/z 1522, $^{DT}CCS_{He}$ = 343.1 Å$^2$ for m/z 2722.[21]

The IM-MS data was processed as described elsewhere.[22] Briefly, $m/z$, arrival times and intensities were extracted for different voltage segments using the IM-MS Browser software (v. B.06.01; Agilent Technologies). The arrival time and signal intensity were extracted for the $m/z$ range of interest (encompassing the isotopic distribution of the non-adducted species) using an in-house R script. The ion mobility peaks were fitted using PeakFit v. 4.11 (Systat Software, San Jose, CA, USA). The proper peak picking and fitting was manually verified. The arrival time at the maximum height of ion mobility peaks was determined for each segment and plotted as a function of

inversed drift voltage $1/\Delta V$. The slope of linear regression line was used to calculate the CCS value ($\Omega$) from Equation (1),

$$t_a = t_0 + \Omega \cdot \left( \frac{L^2 N_0 \frac{T_0 p}{T p_0}}{\frac{3ze}{16}\sqrt{\frac{2\pi}{\mu k_B T}}} \right) \cdot \frac{1}{\Delta V} \quad (1)$$

where $t_a$ is the measured arrival time, $t_0$ is the time spent outside the drift tube and is deduced from the intercept, $L$ length of the mobility cell (78.1 cm), $\mu$ is the reduced mass of the analyte/gas couple, $k_B$ the Boltzmann constant, $T$ the temperature (23.5 ± 1 °C), $p$ the pressure in the drift tube ($p$ = 3.89 ± 1 Torr), $N_0 = 2.687 \times 10^{25} m^{-3}$, $P_0 = 760\ Torr$ and $T_0 = 273.15\ K$. The reconstruction of the experimental CCS distributions from the arrival time distributions at the lowest voltage is then performed using:

$$\Omega = a \cdot \frac{z}{\sqrt{\mu}} t_A \quad (2)$$

where the factor $a$ is determined from the $t_A$ of the peak maximum height at the lowest voltage and Ω calculated from the regression described above, from the peak maximum height.[21]

**Theoretical Collisional Cross Section Calculations**

As there are no available high-resolution structures of recombinant proteins 2S, 3S and 4S, we ran homology modelling of protein structures using SWISS-MODEL.[23] We generated several conformations, compact or extended, by varying the linkers' length using UCSF Chimera v. 1.14.[24] Geometry optimization of the different conformations designed was further performed using MOE 2018.01 software in AMBER99[25] force field (gradient 0.1 kcal/mol/Å$^2$) (see the supporting information Section 2 for detailed information). The theoretical CCS in helium of the geometrically optimized structures were calculated using the trajectory method[26] implemented in Collidoscope.[27]

The most compact conformation of proteins 2S and 3S were generated by performing molecular dynamics (MD) simulation with NAMD 2.14[28] (Win64 multicore CUDA), using the geometrically optimized structures mentioned above as starting material (see the supporting information Section 1 for detailed information). The compact structures in water droplet contained 10 $Na^+$ ($3.5 \times 10^4$ water molecules and $10^5$ atoms in total) and 11 $Na^+$ ($10^4$ water molecules and $3 \times 10^4$ atoms in total) for 2S and 3S, respectively. MD simulations were run over 30 ns and 40 ns for 2S and 3S, respectively (Figure S5). The MD simulation was carried out with Amber99 force field at 450 K after slow heating 25 K/ 100 ps. To overcome the freezing of the system by evaporative cooling we removed from the simulation solvent molecules that have left the droplet after every ~5 ns simulation.[29] In MD simulation we used $Na^+$ as a charge carrier. The NAMD calculations were carried out using graphics processing unit (GPU). Further, semiempirical PM7[30] calculations of the compact structures obtained after MD were conducted using the MOPAC2016 code[31] and CCS calculations were performed using the trajectory method[26] implemented in Collidoscope.[27]

Theoretical lower and upper CCS boundaries for proteins 2S, 3S and 4S were calculated following the procedure described by the Barran's group.[10,32] We assume here that highly compact globular structures result in the lowest CCS limit. The volume of globular proteins is estimated by $V = M_w/\rho$, where ρ is the protein density estimated at 0.904 Da/Å$^3$ (1.5 g/cm$^3$).[33] The radius of a sphere is defined as $r = [3V/(4\pi)]^{1/3}$. The lowest possible CCS is proportional to cross section area of a sphere:

$$CCS_{lower} = 1.19 \times \pi r^2 = 1.19 \times \pi \left(\frac{3V}{4\pi}\right)^{2/3} = 1.19 \times \pi \left(\frac{3M_w}{4\pi\rho}\right)^{2/3} \quad (3)$$

The value 1.19 is an experimentally determined scaling factor for protein mobility in Helium.[34]

The upper limit is calculated based on the assumption that the largest surface corresponds to the most extended, cylinder-like protein structure. Based on Cauchy's theorem, the average projected area of the cylinder is a quarter of its surface area:

$$CCS_{upper} = 1.19 \times \frac{1}{4} \times (2\,\pi r^2 + 2\,\pi r l) \quad (4)$$

A protein with a distance $h = 3.63$ Å between α-carbons will result in length $l = 3.63 \times n$, where $n$ is the number of amino acid residues. The average amino acid ($aa$) radius was calculated assuming that each residue is a cylinder with height $h$, thus $r = [\bar{V}/(\pi h)]^{1/2}$, where $\bar{V} = \sum_i^{aa} \frac{V_i N_i}{n}$. Here, $N_i$ is the number amino acids in the sequence.

**Theoretical solvent accessible surface area (SASA) calculations**

The theoretical solvent accessible surface areas (SASA) were calculated for all generated and optimized protein pdb structures (see Figure 2) using software tool dr_sasa.[35]

**Continuous-flow in-solution HDX IM-MS**

A two-syringe pump (Harvard Apparatus pump 11 Elite for sub-µL flow rate and KD Scientific 78-9100A for several µL flow rates) set-up was used to perform the continuous flow HDX experiments (Figure S6A). The protein sample (100 µM in 15 or 50 mM ammonium acetate solution, pH 6.5) and the diluent (15 or 50 mM ammonium acetate, pD 6.9 (pD = pH +0.4)[36]) containing 98.9 % $D_2O$ (99.9 % D atom, Sigma-Aldrich, France) were pumped at 0.35 and 3.15 µL/min (1:9 ratio), respectively, through PEEK tubing of 0.005-inch ID towards a PEEK high pressure static mixing tee, equipped with a UHMWPE frit (IDEX Health & Science, USA).[37] The H/D exchange took place for 53 sec in the resulting 88.9% deuterated ammonium acetate solution, in a 10.15 cm long 0.0025-inch ID PEEK tubing connecting the mixing tee (swept volume of 2.2 µL) to the ESI source.

To control for gas-phase HDX in the source, gas-phase HDX was also performed by depositing 30 µL of 99.9% $D_2O$ in the ESI chamber (Figure S6B). The IM-MS parameters were similar to those described above, except that the nebulizer value was decreased from 12 to 6 psig to avoid too fast evaporation of the $D_2O$ droplet. It was challenging to maintain a controlled pressure of $D_2O$ vapor in the ESI chamber for an extended period of time. Only data with steady state $m/z$ shifts were used for further processing.

Data processing was different from classical bottom-up or top-down HDX workflows. Isotopic widening is particularly prominent in our experiments because of the protein size and large number

of exchangeable sites, which include side-chains owing to the absence of quenching step and back-exchange reaction. Additionally, adducts for high charge states were poorly resolved. Thus, instead of using peak centroid we opted for calculating the mass shift independently for each charge state, by converting their $m/z$ distribution shift to mass shifts, as proposed by Simmons and Konnerman:[38]

$$\text{Mass shift} = (m/z_{HDX} - m/z_{noHDX}) \times z \quad (5)$$

Protein 3S has 378 aa and 687 exchangeable protons (369 backbone amides, 315 side-chain sites and 3 termini) at pH 6.5. Because the experiment is performed in 88.9 % $D_2O$, the maximum possible mass shift is: $687 \times 0.889 \times (2.014 - 1.008) = 614.407\ Da$.

## Results and Discussions

### Multi-subunit therapeutic proteins adopt multimodal charge state and collision cross section distributions

Here we used native ion mobility MS to analyze recombinant therapeutic proteins currently in advanced clinical trials. Protein 2S (28 kDa, 275 aa) has two subunits, protein 3S (40 kDa 378 aa) has three subunits and protein 4S (56 kDa, 552 aa) has four subunits. All subunits have at least one internal disulfide bridge, and are connected by one 37-aa (2S), two 12-aa (3S) and three 33-aa (4S) disordered linkers. Native MS of these therapeutic multi-subunit proteins shows multimodal CSDs (Figure 1), which usually indicate several folding states in solution. $Na^+$, $NH_4^+$ and acetic acids adducts are visible and in the mass spectra, together with sucrose in the case of protein 3S. The sucrose adducts originate from the formulation buffer used during protein 3S production, which could not be fully removed during buffer exchange. These adducts bind to all charge states, and have the same ion mobilites as their non-adducted counterparts, indicating that they are not specific and thus do not originate from different solution-phase structures.[39]

We made several control experiments to verify whether these multimodal distributions could be due to electrospray effects. Because we observed previously that the CSD of unfolded nucleic acids sequences was mono- or bimodal depending on electrolyte concentration,[22] we compared ESI-MS spectra of protein 3S in 15 or 50 mM $NH_4OAc$ (Figure S1). The charge state distributions were comparable, showing that electrospray charging processes are similar in both conditions. To be closer to the physiological ionic strength, we used 50 mM $NH_4OAc$ for subsequent analyses.

We also investigated the influence of protein concentration to test whether a "charge surplus" or "charge deficiency" regime is governing the charge state distributions.[40] At low protein concentration, the excess charge should suffice to ionize all molecules, while at higher protein concentration, coexisting conformations compete for the available charges and species with more efficient ionization

(usually, unfolded proteins with higher charge states) prevail in the mass spectra.[40] This is the case for protein 4S, less so for protein 3S, and not at all the case for protein 2S (Figure S2). Thus, we should remember that the relative peak areas in the spectra shown below (recorded at 10 µM protein for higher signal-to-noise in ion mobility measurements) do not necessarily reflect the relative abundances of the different conformations in solution.

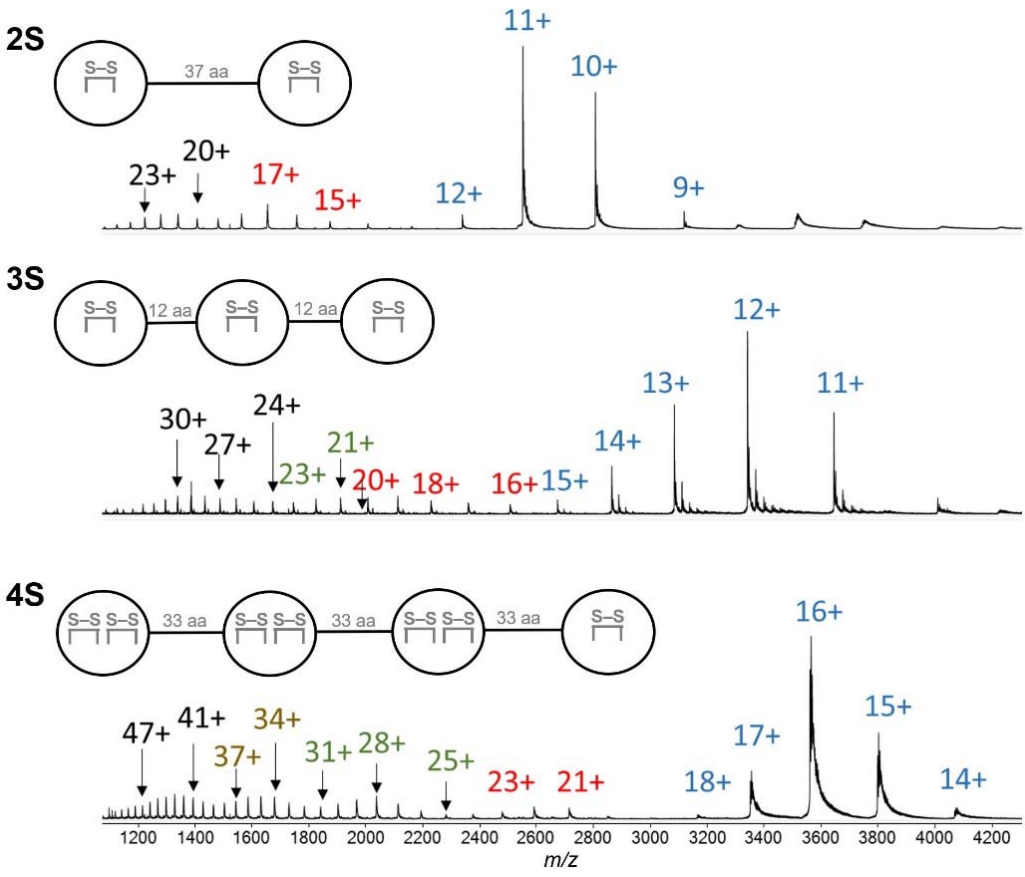


**Figure 1.** Electrospray mass spectra of 10 µM proteins 2S, 3S and 4S in 50 mM $NH_4OAc$ show the presence of at least 3, 4 and 5 charge state distributions (labeled with different colors), respectively. The topology of the proteins is shown in the insets, but for confidentiality reasons we cannot disclose the full amino acid sequences.

The ion mobility data for multi-subunit proteins in 50 mM $NH_4OAc$ corroborate the presence of several conformers of different compactness: 3, 4 and 5 conformational ensembles for proteins 2S, 3S and 4S, respectively (Figure 2). We also studied the influence of pre-IM activation with the fragmentor (a piece of metal that accelerates the ions in the source) to verify that our source conditions were soft enough to avoid collision-induced unfolding (CIU, Figures S3 and S4). The CSDs at low (320 V) and high (500 V) voltages are similar, but using higher fragmentor voltage decreased unspecific adducts (Figure S3), and caused the highest charge states to fragment. According to the CCS distributions, upon collisional activation, the conformers further unfold (Figure S4), meaning that our default source conditions were soft enough to reflect solution structures as closely as possible.

The low charge states (blue) ensemble is very well separated. At the transition between the first two ensembles, $[3S]^{15+}$ adopt two coexisting conformers (see individual CCS distributions in Figure S4). In contrast to these sharp transitions occurring over a single charge state, the shifts between the second, third and further ensembles occur over several charge states, for which the conformers are not so well resolved. The charge state distributions and CCS ensembles are overall better separated for proteins 2S and 4S, which have longer linkers, suggesting that the conformational changes are due to linker extension. We then carried out molecular modeling to better grasp the nature of the conformer ensembles.

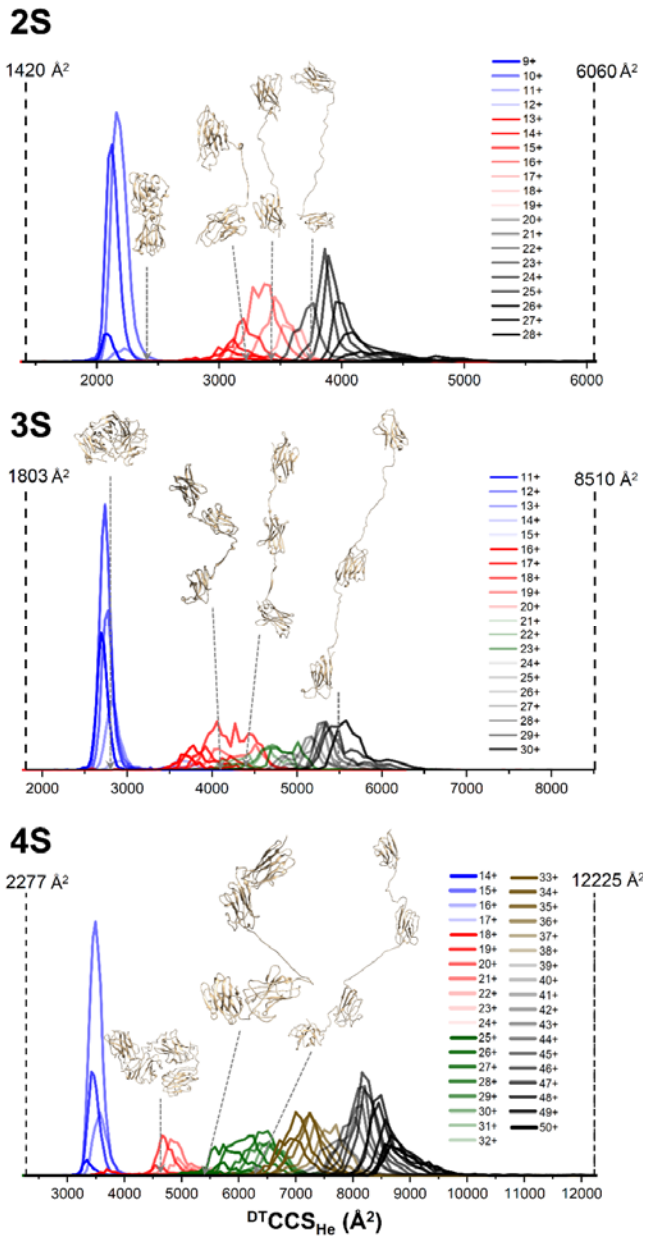


**Figure 2.** Collision cross section distributions of protein ions of different charge states, recorded in 50 mM aqueous $NH_4OAc$. Calculated CCS for structures with compact, normal, extended and elongated linkers candidate structures are indicated by arrows (see CCS values in the supporting information Section 1 and Section 2). The lower and higher extrema correspond to the estimated CCS values of a perfect spherical or a perfectly elongated protein of the same size.

**Ion mobility measurements suggest that gas-phase conformations differ by linker extension**

We first estimated the CCS extrema of our proteins, by assuming that the smallest corresponds to a sphere and the largest to a linearized structure.[10,32] These boundaries (vertical dotted lines, Fig. 2) show that none of the observed structures reach a complete compaction or extension in the gas phase.

Since disulfide bridges rigidify each protein subunit, the most likely difference between these conformations resides in the linkers. To test this hypothesis, we generated compact and extended conformation by varying the linkers' extension (see supporting information Section 1 and Section 2). However, we could not match the most compact CCSs by just varying the linkers' distances, and this suggests a closer packing of the subunits. We thus ran MD simulations of 2S and 3S in droplets for 30 and 40 ns, respectively (Figure S5). Then we optimized the compact structures in the gas phase at the semiempirical PM7[30] level to avoid any bias related to using force fields.[41] The results confirm that the lowest charge states (blue distribution) have a globular conformation with the close packing of the subunits.

The structures with one or two extended linkers match well with the next CCS distributions (red and green in Figure 2). However, none of these candidate structures matches with the experimental CCS values of the most extended conformers (black ensembles). We supposed that this further extension could result from subunit unfolding, in the region not stapled by disulfide bridges. We thus generated further candidate structures, wherein both the linkers and the subunits before their disulfide bridge staple are unfolded and extended, by adjusting torsions using UCSF Chimera v. 1.14 followed by geometry optimization. The theoretical CCS value of this candidate structure with 'elongated' linkers match well the largest experimental CCS distributions.

In summary, gas-phase conformations correspond to a globular form and beads-on-a-string conformations with various linker extensions. For the highest charge states, the extremities of the subunits are also extended. However, gas-phase conformations can be affected by either compaction

due to the charged residue mechanism for the lowest charge states,[42] or (Coulomb) force pulling for the highest charge state.

**Charge state and collision cross section distributions indicate different folding states in solution**

Inspired by earlier work,[43] we coupled HDX with native IM-MS to verify whether the multiple gas-phase ensembles reflect multiple ensembles in solution. We tested this on protein 3S. After continuous labeling with $D_2O$, the protein in 50 mM $NH_4OAc$ solution and 88.9 % $D_2O$ is directly electrosprayed at room temperature, without any quenching step that would denature the protein (Figure S6A). If multiple protein conformations are present in solution and if they inter-convert slowly compared to the labeling time, we expect to observe different levels of deuterium uptake for different CSD and CCS ensembles. In contrast to typical contemporary HDX experiments, the absence of quenching and LC separation in $H_2O$ implies that amide, side-chain and termini protons are all exchangeable without solution-phase back exchange, but we would expect some amide protons to remain protected.

Figure S7 shows the mass spectra recorded without (Figure S8) and with H/D exchange. The maximum possible mass shift is $614.4\ Da$. Figure 3A groups the mass shift plots after 53 seconds of HDX per family: the shifts are on average 383 Da for the lowest charged ions (11+—13+; 14+ and 15+ have poor signal-to-noise ratio), 396 Da for the second group (16+—19+), 410 Da for the third group (20+—24+) and 448 Da for the most highly charged ions (27+—30+). The shifts are larger than simply the difference in the number of protons between charge states. We also notice that the increment is larger between the third and fourth groups ($\Delta m$ = 38 Da) than between the three first groups ($\Delta m$ = 13 and 14 Da), which is in line with the molecular modeling suggesting further extension and deprotection within the subunits in the last group. Many sites are not exchanged even

for the most extended group (~ 186 sites for 27+—30+), consistent with (at least partial) conservation of subunit folding. For more compact conformers, the differences in uptake suggest some interactions occur between subunits, assuming their folding remains unchanged.

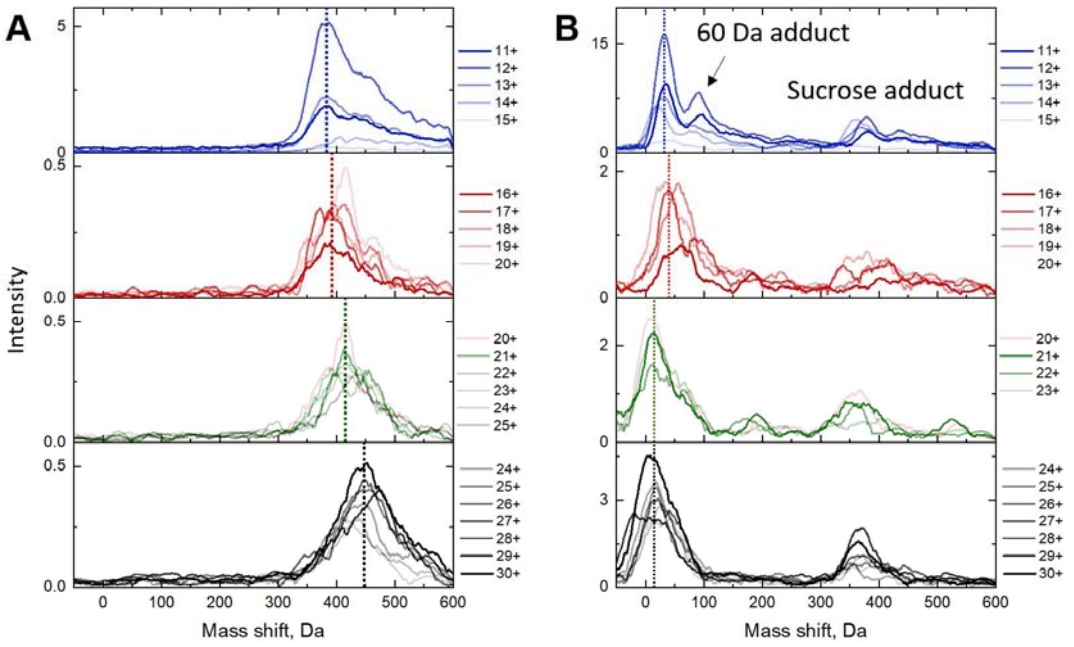


**Figure 3. (A)** Solution HDX (53 s) and **(B)** gas-phase HDX mass shifts for different charge states of protein **3S**. The charge state grouping and color code is the same as in Figures 1 and 2. The vertical dashed lines indicate the average mass shift.

Our results suggest that the different conformations detected in the gas phase reflect different solution folding states. Yet this conclusion is valid only if the difference in HDX is due to solution and not gas-phase HDX. Indeed, we electrospray here proteins from solutions with large $D_2O$ concentrations at 3.5 µL/min, so the exchange may occur partially or entirely with $D_2O$ vapors in the source. To test the direction of the shift in gas-phase HDX, we performed IM-MS experiments by spraying protein 3S in water and doping the source atmosphere with $D_2O$ (see supplementary Figure

S6B for experimental details). The mass spectrum of protein 3S with gas phase HDX IM-MS (Figure S9) resembles those presented in Figure 1. Figure 3B shows low levels of deuteration in the gas-phase compared to solution-phase HDX. The differences between charge states are small, and the gas-phase deuteration is more extensive for the lower charge states. This is in line with the relay mechanism, according to which gas-phase deuterium exchange require $D_2O$ to simultaneously make hydrogen bonds between a protonated site and a carbonyl oxygen, and is thus more favorable for folded states.[44] Most importantly for our discussion, the charge state dependence of gas-phase HDX is the opposite to the one observed for the solution-phase HDX experiments, proving that the multiple conformations detected in the charge state and collision cross section distributions reflect solution protein conformational ensembles. High charge states show both the largest extent of HDX and CCS values suggesting extension of the extremities of the subunits in the regions not protected by disulfide bridges. We deduce that some force pulling occurred in the presence of solvent, but it is still unclear whether it reflects bulk solution unfolding or a rapid process in the late stages of charge state acquisition.

**Electrospray ionization via a bead ejection mechanism (BEM)**

To compare the extent of unfolding as a function of the charge state for the three proteins, Figure 4A plots reduced CCS values as a function of reduced charge state, defined as follows: (1) the reduced CCS is the average experimental CCS divided by $CCS_0$, the CCS of a hypothetical spherical protein of the same weight with maximum density (see Figure 2); (2) the reduced charge is the observed charge divided by the Rayleigh limit charge of the same hypothetical spherical protein (assuming $\gamma$ = 0.072 J m$^{-3}$, water at 25°C). This gives $z_R$ = 12.3 for 2S, $z_R$ = 14.7 for 3S and $z_R$ = 17.5 for 4S. Given that the $CCS_0$ is significantly lower than the smallest experimental CCS, $z_R$ is likely underestimated too. Nevertheless, we see a clear jump in reduced CCS when the experimental charge becomes higher than the Rayleigh limit. This is in line with the first ensemble (blue in Figures 1-2) being ionized

purely via the charged residue mechanism (CRM) and resulting in a globular ensemble, while the other ensembles are ionized via a different mechanism.

Next, we wanted to compare unfolding as a function of the charge state with known trends for globular and unfolded or disordered proteins. We used correlations that relate the charge state with the solvent accessible surface area (SASA) in a ln/ln plot (Figure 4B).[45,19] These correlations (lines in Figure 4B) were established by calculating the SASA from published atomic coordinates of known proteins, and correlating it with the average charge state observed in ESI-MS. Our approach is different because we don't have solution structures, but we have generated several gas-phase molecular models. We thus calculated the SASA of our gas-phase models and we assigned the corresponding charge state as the one with the experimental CCS best matching their theoretical CCS (note that this may differ from the charge used during the molecular modeling procedure). Figure 4B compares each model to the trend lines for globular and unfolded proteins.

Our most compact models lie slightly above the trend line for globular proteins, but that is unsurprising given that the subunits are ellipsoidal rather than spherical. More interesting is the positioning of the beads-on-a-string models compared with the trend line established for fully unfolded or intrinsically disordered proteins. Data points are below and above the trend line. Those most clearly below have not all linkers extended ($[3S]^{18+}$, $[4S]^{20+}$), while those most clearly above are the models with linear extension of the linker and part of the subunits ($[2S]^{21+}$, $[3S]^{28+}$). The beads-on-a-string structures thus behave similarly to fully unfolded or intrinsically disordered proteins, although their topology is clearly different (the domains remain globular while the linkers are stretched).

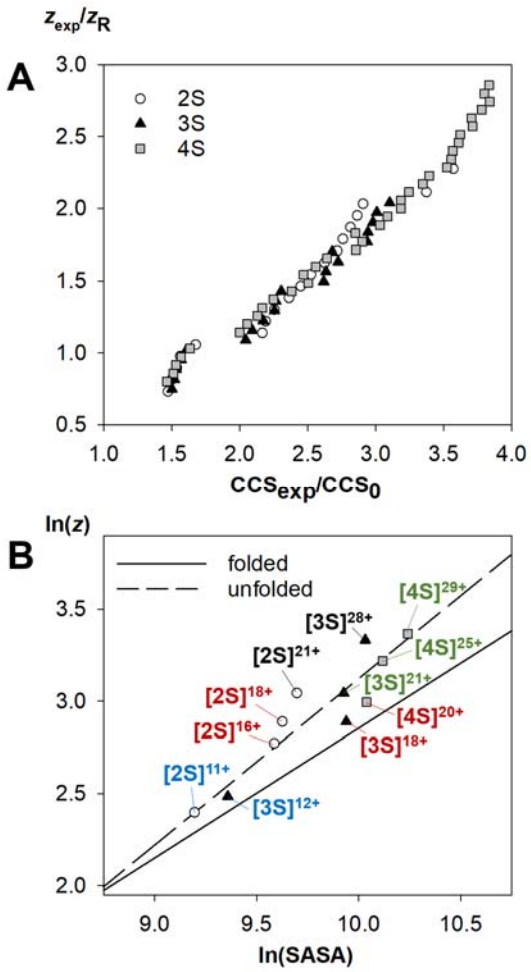


**Figure 4. (A)** Experimental charge ($z_{exp}$) divided by predicted Rayleigh charge ($z_R$) of a spherical protein of that size vs. experimental CCS divided by $CCS_0$ of predicted spherical protein of the same size. **(B)** Correlation between charge and solvent accessible surface area (SASA). The solid line corresponds to SASA vs average charge state for globular[45] and dash line to intrinsically disordered proteins[19]. The symbols correspond to the SASA of the molecular models presented in Figure 2, with the charge state of the corresponding CCS. The color coding corresponds to the ensembles defined in Figures 1-2.

The lesson learned is that the globular trend line predicts well the highest charge attainable through the charged residue mechanism, but the unfolded trend line does not inform on the type of folding or unfolding. Instead, the acquisition of higher charge states indicates that another electrospray mechanism than the CRM has occurred. For proteins, the only alternative to CRM proposed to date is the chain ejection mechanism (CEM), usually pictured as a single chain extruded from the parent droplet. But although the CEM is plausible for unstructured proteins or polymers, it is not fully applicable to our multi-subunit proteins. We thus propose an intermediate "bead ejection" mechanism (BEM; Figure 5), which can be viewed as the coexistence between the CRM and CEM: subunits can remain folded with a solvent layer around them defining a local CRM-like environment, while linkers extend via a CEM-like process. The main difference is that entire subunits can be ejected from the parent droplet.

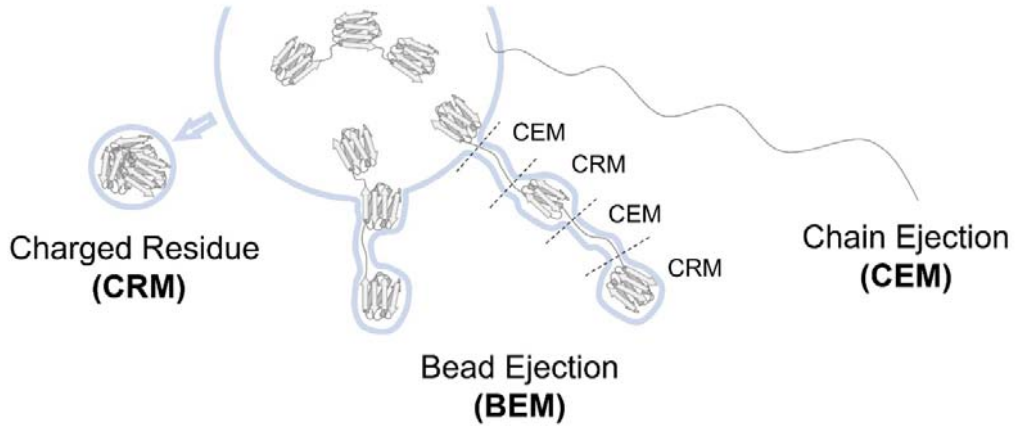


**Figure 5.** Illustration of the proposed coexisting ion charging mechanisms: the charged residue mechanism (CRM) produces a globular ensemble, charged close to the Rayleigh limit. Pure chain ejection mechanism (CEM) produces a fully extended conformation. The bead ejection mechanism (BEM) is intermediate because it is a composite of the CRM and the CEM: folded domains can be ionized by the CRM while disordered regions can be ionized by the CEM. Both the CRM and CEM can reflect native conformations.

Such “beads on a string” or “pearl” mechanism has been proposed before in electrospray for synthetic polymers.[46–48] We propose it provides the missing scenario in the protein ionization mechanisms, for all intermediate charge states not leading to a fully stretched conformation. Interestingly, several molecular models proposed to match the CCS of intermediate charge states of denatured or disordered proteins actually have a beads on a string topology.[11,49,50] Given that most fully denatured or fully intrinsically disordered proteins give a charge/SASA relationship matching that of our multi-subunit proteins, denatured or intrinsically disordered proteins could very well be ionized according to a bead ejection mechanism. The key difference is that our protein systems have beads and linkers clearly delimited by the sequence, and thus result in multimodal charge state and CCS distributions, whereas fully unstructured (bio)polymers can end up in a continuum of charge states and conformations, as beads can form anywhere and be of any size.

## Conclusions

The lessons learned from our electrospray ion mobility mass spectrometry study of multi-subunit therapeutic proteins in native conditions are:

1. Multimodal charge state distributions can appear when the subunits do not interact tightly in solution, otherwise all the population would follow the charged residue mechanism. Yet solution HDX suggests the subunits can interact to some extent, yielding several conformational states coexisting in solution and leading to distinct charge state ensembles.
2. Multimodal charge state distributions are better separated when the disordered linkers are long. The multimodal charge state distribution is mirrored in a multimodal CCS distribution. The linker size effect may explain why such multimodal CSDs were not reported before with multi-subunit proteins such as polyubiquitins[51] or full antibodies[52] (moreover, the three domains of monoclonal antibodies are not arranged like pearls on a necklace).

3. Only the lowest charge state and CCS distributions are compatible with ionization via the charged residue mechanism (CRM). We suggest that higher charge states can be ionized via a bead ejection mechanism, wherein each subunit stays native and follows the CRM, while the linkers extend and follow the CEM. The subunits are ejected from the parent droplet like beads on a string. We coin this intermediate electrospray mechanism the "bead ejection mechanism" (BEM).
4. The BEM is unavoidable in our molecular system because the inner disulfide bridges within subunits render full CEM impossible. However, we argue that the BEM is also a reasonable scenario for the formation of intermediate charge states of other polymers and biopolymers. Future experimental work will be devoted to testing how general this model can be. Molecular modeling could also bring important mechanistical insight, especially on the balance of forces during the BEM. In the long run, this could enable one to predict charge state distributions and CCS distributions based on the sequence and supposed solution structures.

## Acknowledgements

We acknowledge funding for this project by the ANR (ANR-18-CE29-0013-POLYnESI grant to VG) and the Conseil Régional Nouvelle Aquitaine (PROMIS project to VG).

## Supplementary information

Additional mass spectra and collision cross section distributions as described in the text, snapshots of MD simulations, supplementary experimental details on the HDX/MS setups and protocols used for protein structure generation with compact, normal, extended and elongated linkers (PDF).

## References


(1) Yamashita, M.; Fenn, J. B. Electrospray Ion Source. Another Variation on the Free-Jet Theme. *J Phys.Chem.* **1984**, *88* (20), 4451–4459. https://doi.org/10.1021/j150664a002.

(2) Fenn, J. B.; Mann, M.; Meng, C. K.; Wong, S. F.; Whitehouse, C. M. Electrospray Ionization for Mass Spectrometry of Large Biomolecules. *Science.* **1989**, *246* (4926), 64–71. https://doi.org/10.1126/science.2675315.

(3) Cole, R. B. Some Tenets Pertaining to Electrospray Ionization Mass Spectrometry. *J. Mass Spectrom.* **2000**, *35* (7), 763–772. https://doi.org/10.1002/1096-9888(200007)35:7<763::AID-JMS16>3.0.CO;2-#.

(4) Kebarle, P. A Brief Overview of the Present Status of the Mechanisms Involved in Electrospray Mass Spectrometry. *J. Mass Spectrom.* **2000**, *35* (7), 804–817. https://doi.org/10.1002/1096-9888(200007)35:7<804::AID-JMS22>3.0.CO;2-Q.

(5) Iribarne, J. V. On the Evaporation of Small Ions from Charged Droplets. *J. Chem. Phys.* **1976**, *64* (6), 2287. https://doi.org/10.1063/1.432536.

(6) Wang, G.; Cole, R. B. Charged Residue versus Ion Evaporation for Formation of Alkali Metal Halide Cluster Ions in ESI. *Anal. Chim. Acta* **2000**, *406* (1), 53–65. https://doi.org/10.1016/S0003-2670(99)00599-1.

(7) Dole, M.; Mack, L. L.; Hines, R. L.; Mobley, R. C.; Ferguson, L. D.; Alice, M. B. Molecular Beams of Macroions. *J. Chem. Phys.* **1968**, *49* (5), 2240–2249. https://doi.org/10.1063/1.1670391.

(8) Fernandez De La Mora, J. Electrospray Ionization of Large Multiply Charged Species Proceeds via Dole's Charged Residue Mechanism. *Anal. Chim. Acta* **2000**, *406* (1), 93–104. https://doi.org/10.1016/S0003-2670(99)00601-7.

(9) Konermann, L.; Ahadi, E.; Rodriguez, A. D.; Vahidi, S. Unraveling the Mechanism of Electrospray Ionization. *Anal. Chem.* **2013**, *85* (1), 2–9. https://doi.org/10.1021/ac302789c.

(10) Beveridge, R.; Covill, S.; Pacholarz, K. J.; Kalapothakis, J. M. D.; MacPhee, C. E.; Barran, P. E. A Mass-Spectrometry-Based Framework To Define the Extent of Disorder in Proteins. *Anal. Chem.* **2014**, *86* (22), 10979–10991. https://doi.org/10.1021/ac5027435.

(11) Beveridge, R.; Phillips, A. S.; Denbigh, L.; Saleem, H. M.; MacPhee, C. E.; Barran, P. E. Relating Gas Phase to Solution Conformations: Lessons from Disordered Proteins. *Proteomics* **2015**, *15* (16), 2872–2883. https://doi.org/10.1002/pmic.201400605.

(12) Usmani, S. S.; Bedi, G.; Samuel, J. S.; Singh, S.; Kalra, S.; Kumar, P.; Ahuja, A. A.; Sharma, M.; Gautam, A.; Raghava, G. P. S. THPdb: Database of FDA-Approved Peptide and Protein Therapeutics. *PLoS One* **2017**, *12* (7), 1–12. https://doi.org/10.1371/journal.pone.0181748.

(13) Fenn, J. B. Ion Formation from Charged Droplets: Roles of Geometry, Energy, and Time. *J. Am. Soc. Mass Spectrom.* **1993**, *4* (7), 524–535. https://doi.org/10.1016/1044-0305(93)85014-O.

(14) Konermann, L.; Douglas, D. J. Acid-Induced Unfolding of Cytochrome *c* at Different Methanol Concentrations: Electrospray Ionization Mass Spectrometry Specifically Monitors Changes in the Tertiary Structure. *Biochemistry* **1997**, *36* (40), 12296–12302. https://doi.org/10.1021/bi971266u.

(15) Dobo, A.; Kaltashov, I. A. Detection of Multiple Protein Conformational Ensembles in Solution via Deconvolution of Charge-State Distributions in ESI MS. *Anal. Chem.* **2001**, *73*

(20), 4763–4773. https://doi.org/10.1021/ac010713f.

(16) Li, J.; Santambrogio, C.; Brocca, S.; Rossetti, G.; Carloni, P.; Grandori, R. Conformational Effects in Protein Electrospray-Ionization Mass Spectrometry. *Mass Spectrom. Rev.* **2016**, *35* (1), 111–122. https://doi.org/10.1002/mas.21465.

(17) Clemmer, D. E.; Jarrold, M. F. Ion Mobility Measurements and Their Applications to Clusters and Biomolecules. *J. Mass Spectrom.* **1997**, *32* (6), 577–592. https://doi.org/10.1002/(SICI)1096-9888(199706)32:6<577::AID-JMS530>3.0.CO;2-4.

(18) Kanu, A. B.; Dwivedi, P.; Tam, M.; Matz, L.; Hill, H. H. Ion Mobility-Mass Spectrometry. *J. Mass Spectrom.* **2008**, *43* (1), 1–22. https://doi.org/10.1002/jms.1383.

(19) Testa, L.; Brocca, S.; Grandori, R. Charge-Surface Correlation in Electrospray Ionization of Folded and Unfolded Proteins. *Anal. Chem.* **2011**, *83* (17), 6459–6463. https://doi.org/10.1021/ac201740z.

(20) Gabelica, V.; Livet, S.; Rosu, F. Optimizing Native Ion Mobility Q-TOF in Helium and Nitrogen for Very Fragile Noncovalent Structures. *J. Am. Soc. Mass Spectrom.* **2018**, *29* (11), 2189–2198. https://doi.org/10.1007/s13361-018-2029-4.

(21) Marchand, A.; Livet, S.; Rosu, F.; Gabelica, V. Drift Tube Ion Mobility: How to Reconstruct Collision Cross Section Distributions from Arrival Time Distributions? *Anal. Chem.* **2017**, *89* (23), 12674–12681. https://doi.org/10.1021/acs.analchem.7b01736.

(22) Khristenko, N.; Amato, J.; Livet, S.; Pagano, B.; Randazzo, A.; Gabelica, V. Native Ion Mobility Mass Spectrometry: When Gas-Phase Ion Structures Depend on the Electrospray Charging Process. *J. Am. Soc. Mass Spectrom.* **2019**, *30* (6), 1069–1081. https://doi.org/10.1007/s13361-019-02152-3.

(23) Waterhouse, A.; Bertoni, M.; Bienert, S.; Studer, G.; Tauriello, G.; Gumienny, R.; Heer, F. T.; De Beer, T. A. P.; Rempfer, C.; Bordoli, L.; Lepore, R.; Schwede, T. SWISS-MODEL: Homology Modelling of Protein Structures and Complexes. *Nucleic Acids Res.* **2018**, *46* (W1), W296–W303. https://doi.org/10.1093/nar/gky427.

(24) Pettersen, E. F.; Goddard, T. D.; Huang, C. C.; Couch, G. S.; Greenblatt, D. M.; Meng, E. C.; Ferrin, T. E. UCSF Chimera—A Visualization System for Exploratory Research and Analysis. *J. Comput. Chem.* **2004**, *25* (13), 1605–1612. https://doi.org/10.1002/jcc.20084.

(25) Lindorff-Larsen, K.; Piana, S.; Palmo, K.; Maragakis, P.; Klepeis, J. L.; Dror, R. O.; Shaw, D. E. Improved Side-Chain Torsion Potentials for the Amber Ff99SB Protein Force Field. *Proteins Struct. Funct. Bioinforma.* **2010**, *78* (8), 1950–1958. https://doi.org/10.1002/prot.22711.

(26) Mesleh, M. F.; Hunter, J. M.; Shvartsburg, A. A.; Schatz, G. C.; Jarrold, M. F. Structural Information from Ion Mobility Measurements: Effects of the Long-Range Potential. *J. Phys. Chem.* **1996**, *100* (40), 16082–16086. https://doi.org/10.1021/jp961623v.

(27) Ewing, S. A.; Donor, M. T.; Wilson, J. W.; Prell, J. S. Collidoscope: An Improved Tool for Computing Collisional Cross-Sections with the Trajectory Method. *J. Am. Soc. Mass Spectrom.* **2017**, *28* (4), 587–596. https://doi.org/10.1007/s13361-017-1594-2.

(28) Phillips, J. C.; Hardy, D. J.; Maia, J. D. C.; Stone, J. E.; Ribeiro, J. V.; Bernardi, R. C.; Buch, R.; Fiorin, G.; Hénin, J.; Jiang, W.; McGreevy, R.; Melo, M. C. R.; Radak, B. K.; Skeel, R. D.; Singharoy, A.; Wang, Y.; Roux, B.; Aksimentiev, A.; Luthey-Schulten, Z.; Kalé, L. V.; Schulten, K.; Chipot, C.; Tajkhorshid, E. Scalable Molecular Dynamics on CPU and GPU Architectures with NAMD. *J. Chem. Phys.* **2020**, *153* (4), 044130. https://doi.org/10.1063/5.0014475.

(29) Konermann, L.; Metwally, H.; McAllister, R. G.; Popa, V. How to Run Molecular Dynamics

Simulations on Electrospray Droplets and Gas Phase Proteins: Basic Guidelines and Selected Applications. *Methods* **2018**, *144*, 104–112. https://doi.org/10.1016/j.ymeth.2018.04.010.

(30) Stewart, J. J. P. Optimization of Parameters for Semiempirical Methods VI: More Modifications to the NDDO Approximations and Re-Optimization of Parameters. *J. Mol. Model.* **2013**, *19* (1), 1–32. https://doi.org/10.1007/s00894-012-1667-x.

(31) Stewart, J. J. P. MOPAC2016. *Stewart Comput. Chem.* **2016**, *Colorado Springs, CO, USA*. HTTP://OpenMOPAC.net

(32) Beveridge, R.; Migas, L. G.; Das, R. K.; Pappu, R. V.; Kriwacki, R. W.; Barran, P. E. Ion Mobility Mass Spectrometry Uncovers the Impact of the Patterning of Oppositely Charged Residues on the Conformational Distributions of Intrinsically Disordered Proteins. *J. Am. Chem. Soc.* **2019**, *141* (12), 4908–4918. https://doi.org/10.1021/jacs.8b13483.

(33) Fischer, H.; Polikarpov, I.; Craievich, A. F. Average Protein Density Is a Molecular-Weight-Dependent Function. *Protein Sci.* **2009**, *13* (10), 2825–2828. https://doi.org/10.1110/ps.04688204.

(34) Fernandez de la Mora, J. Electrospray Ionization of Large Multiply Charged Species Proceeds via Dole's Charged Residue Mechanism. *Anal. Chim. Acta* **2000**, *406* (1), 93–104. https://doi.org/10.1016/S0003-2670(99)00601-7.

(35) Ribeiro, J.; Ríos-Vera, C.; Melo, F.; Schüller, A. Calculation of Accurate Interatomic Contact Surface Areas for the Quantitative Analysis of Non-Bonded Molecular Interactions. *Bioinformatics* **2019**, *35* (18), 3499–3501. https://doi.org/10.1093/bioinformatics/btz062.

(36) Glasoe, P. K.; Long, F. A. Use of Glass Electrodes to Measure Acidities in Deuterium Oxide. *J. Phys. Chem.* **1960**, *64* (1), 188–190. https://doi.org/10.1021/j100830a521.

(37) Largy, E.; Gabelica, V. Native Hydrogen/Deuterium Exchange Mass Spectrometry of Structured DNA Oligonucleotides. *Anal. Chem.* **2020**, *92* (6), 4402–4410. https://doi.org/10.1021/acs.analchem.9b05298.

(38) Simmons, D. A.; Konermann, L. Characterization of Transient Protein Folding Intermediates during Myoglobin Reconstitution by Time-Resolved Electrospray Mass Spectrometry with on-Line Isotopic Pulse Labeling. *Biochemistry* **2002**, *41* (6), 1906–1914. https://doi.org/10.1021/bi011697j.

(39) Kebarle, P.; Verkerk, U. H. Electrospray: From Ions in Solution to Ions in the Gas Phase, What We Know Now. *Mass Spectrom. Rev.* **2009**, *28* (6), 898–917. https://doi.org/10.1002/mas.20247.

(40) Kuprowski, M. C.; Konermann, L. Signal Response of Coexisting Protein Conformers in Electrospray Mass Spectrometry. *Anal. Chem.* **2007**, *79* (6), 2499–2506. https://doi.org/10.1021/ac0620056.

(41) Rolland, A. D.; Prell, J. S. Computational Insights into Compaction of Gas-Phase Protein and Protein Complex Ions in Native Ion Mobility-Mass Spectrometry. *TrAC Trends Anal. Chem.* **2019**, *116*, 282–291. https://doi.org/10.1016/j.trac.2019.04.023.

(42) Devine, P. W. A.; Fisher, H. C.; Calabrese, A. N.; Whelan, F.; Higazi, D. R.; Potts, J. R.; Lowe, D. C.; Radford, S. E.; Ashcroft, A. E. Investigating the Structural Compaction of Biomolecules Upon Transition to the Gas-Phase Using ESI-TWIMS-MS. *J. Am. Soc. Mass Spectrom.* **2017**, *28* (9), 1855–1862. https://doi.org/10.1007/s13361-017-1689-9.

(43) Hossain, B. M.; Konermann, L. Pulsed Hydrogen/Deuterium Exchange MS/MS for Studying the Relationship between Noncovalent Protein Complexes in Solution and in the Gas Phase after Electrospray Ionization. *Anal. Chem.* **2006**, *78* (5), 1613–1619. https://doi.org/10.1021/ac051687e.

(44) Campbell, S.; Rodgers, M. T.; Marzluff, E. M.; Beauchamp, J. L. Deuterium Exchange Reactions as a Probe of Biomolecule Structure. Fundamental Studies of Gas Phase H/D Exchange Reactions of Protonated Glycine Oligomers with $D_2O$, $CD_3OD$, $CD_3CO_2D$, and $ND_3$. *J. Am. Chem. Soc.* **1995**, *117* (51), 12840–12854. https://doi.org/10.1021/ja00156a023.

(45) Kaltashov, I. A.; Mohimen, A. Estimates of Protein Surface Areas in Solution by Electrospray Ionization Mass Spectrometry. *Anal. Chem.* **2005**, *77* (16), 5370–5379. https://doi.org/10.1021/ac050511+.

(46) Ude, S.; Fernández de la Mora, J.; Thomson, B. A. Charge-Induced Unfolding of Multiply Charged Polyethylene Glycol Ions. *J. Am. Chem. Soc.* **2004**, *126* (38), 12184–12190. https://doi.org/10.1021/ja0381306.

(47) Larriba, C.; Fernandez De La Mora, J. The Gas Phase Structure of Coulombically Stretched Polyethylene Glycol Ions. *J. Phys. Chem. B* **2012**, *116* (1), 593–598. https://doi.org/10.1021/jp2092972.

(48) Consta, S.; Malevanets, A. Classification of the Ejection Mechanisms of Charged Macromolecules from Liquid Droplets. *J. Chem. Phys.* **2013**, *138* (4), 044314. https://doi.org/10.1063/1.4789018.

(49) Clemmer, D. E.; Hudgins, R. R.; Jarrold, M. F. Naked Protein Conformations: Cytochrome c in the Gas Phase. *J. Am. Chem. Soc.* **1995**, *117* (40), 10141–10142. https://doi.org/10.1021/ja00145a037.

(50) Vahidi, S.; Stocks, B. B.; Konermann, L. Partially Disordered Proteins Studied by Ion Mobility-Mass Spectrometry: Implications for the Preservation of Solution Phase Structure in the Gas Phase. *Anal. Chem.* **2013**, *85* (21), 10471–10478. https://doi.org/10.1021/ac402490r.

(51) Zhong, Y.; Han, L.; Ruotolo, B. T. Collisional and Coulombic Unfolding of Gas-Phase Proteins: High Correlation to Their Domain Structures in Solution. *Angew. Chemie Int. Ed.* **2014**, *53* (35), 9209–9212. https://doi.org/10.1002/anie.201403784.

(52) Pacholarz, K. J.; Porrini, M.; Garlish, R. A.; Burnley, R. J.; Taylor, R. J.; Henry, A. J.; Barran, P. E. Dynamics of Intact Immunoglobulin G Explored by Drift-Tube Ion-Mobility Mass Spectrometry and Molecular Modeling. *Angew. Chemie Int. Ed.* **2014**, *53* (30), 7765–7769. https://doi.org/10.1002/anie.201402863.